PARTICLE TECHNOLOGY AND FLUIDIZATION

Journal Section

Fluidization of wet cohesive powder in virtual Couette rheometer

Sudeshna Roy[1,2†] | Chongqiang Zhu[1,3] | Ilaria Rucco[1] | Raffaella Ocone[1]

[1]School of Engineering and Physical Sciences,, Heriot-Watt University, Edinburgh, EH144AS, UK

[2]Institute for Multiscale Simulation, Friedrich-Alexander-Universität Erlangen-Nürnberg, Cauerstraße 3, 91058 Erlangen, Germany

[3]School of Science and Engineering, University of Dundee, Dundee, DD14HN, UK

Correspondence
Institute for Multiscale Simulation, Friedrich-Alexander-Universität Erlangen-Nürnberg, Cauerstraße 3, 91058 Erlangen, Germany
Email: sudeshna.roy@fau.de

Present address
[†]Institute for Multiscale Simulation, Friedrich-Alexander-Universität Erlangen-Nürnberg, Cauerstraße 3, 91058 Erlangen, Germany

Funding information
Engineering and Physical Sciences Research Council, Grant/Award Number: EP

We use a virtual Couette rheometer to study the behaviour of dry and wet granular materials in aerated bed. A typical fluidization curve for dry powders exhibits fixed bed characterized by linear increase in pressure drop with increasing air velocity. This is followed by a fluidized bed at a constant pressure drop with further increase in air velocity. However, wet powders display different aeration behaviour due to the inhomogeneous gas flow through the bed. The fluidization behaviour of the powder upon addition of small amounts of silicon oil liquid has been tested for two different grain sizes. We distinguish different regimes of fluidization for wet powders with different saturation of silicon oil and different grain sizes. Further, we compare the hysteresis effects in fluidization and de-fluidization cycles of the materials. We also compare the shear stresses and study the rheology of the materials under different fluidized condition.

KEYWORDS
fluidization, *cohesion*, hysteresis, rheology

1 | INTRODUCTION

Fine and ultrafine powders have recently received growing interest in both industrial and academic sectors due to their very distinctive features, mainly coming from their very small primary particle size and very large surface-to-volume ratio. Indeed, due to these characteristics, they can provide better contact efficiency and higher re-

action rates per unit volume of reactor than traditional materials in the case of gas/solid and solid/solid reactions. They have been used to produce a large variety of materials, such as catalysts, sorbents, cosmetics, etc. Therefore, the interest in using this type of granular materials in a variety of industrial processes raises many questions about how they can be handled and processed in large scale applications. Among many available techniques for continuously handling and dispersing granular solids, gas fluidization is one of the most efficient one used in industries, mainly due to the large gas–solid contact area. One goal of this article is to distinguish fluidization behaviour between dry non-cohesive and wet cohesive powder materials.

Typical fluidization and de-fluidization curves for dry powders show that loading and unloading curves follow one another closely; only a slight hysteresis effect is evident in some cases [22, 23]. Relatively small changes in saturation of interstitial liquid can transform a fine free-flowing powder into one which is cohesive. The liquid capillary bridges formed connecting grains can alter the physical properties of the granular materials dramatically. The attractive forces between the particles connected by bridges in the micro scale result in increasing bulk cohesion for moderately saturated materials. This prompts us to investigate the influence of liquid saturation on fluidization and de-fluidization behaviour of powder materials. For too much liquid, the capillary bridges start to merge, and they eventually disappear altogether when the powder is fully saturated. Hence, the materials behave presumably different when saturation is increased. Thus, we investigate the fluidization and de-fluidization behaviour of powders for dry non-cohesive powders and wet cohesive powders with lower to intermediate saturation of liquid.

The behavior of dry granular materials in the static aerated bed has been investigated in several studies. Klien et al. developed an annular shear to shear limestone powders at various normal pressures and shear velocities ranging from 0.07 to 4200 mm/min [8]. This device enables the study of aerated sample under constant pressure. The results show that the shear stress is independent of aeration condition upto a fluidization index of 0.7 while it decreases with increasing air velocity for higher fluidization index. A rotational shear tester for aerated shear flow as built by Barletta et al. by modifying the Peschl shear tester was used to investigate the impact of aeration on the flow behaviour of cohesive powders e.g. silica and magnesium carbonate [10]. This study shows that the aeration does impact the friction coefficient of the materials below a critical fluidization index (< 0.7) in the quasistatic regime. Similar rheology studies were done by Bruni et al. [11] and Tomasetta et al. [16] in a mechanically stirred fluidized bed for aerated glass beads and silica powders. Salehi et al. used the Anton Paar powder cell to measure the torque necessary to rotate a flat impeller in beds of glass beads, sand and alumina powders aerated between no aeration to the fluidization limit [20]. The experimental results showed that the measured torques depend on the material tested, applied airflow rate, impeller depth, and the height of the impeller blade. Zhu et al. studied the dynamic characteristics of cohesive granular materials discharged from hopper under modulated pulsed airflow [25]. A different experimental configuration with the coaxial cylinder viscometer was also used in a number of studies to investigate the particles stress in aerated and fluidized beds. The shear stress here is computed from the torque, T, needed to move the rotating cylinder through the material [4, 5].

Partially saturated granular materials with liquid bridges between particle pairs lead to the formation of tensile forces. The tensile forces generated at particle level result in cohesion at macroscopic scale, leading to additional shear stresses to rotate the impeller in unsaturated granular bed. This also directly influences the viscosity of the flowing materials. Thus, the interstitial liquid for unsaturated granular materials play a critical role on the rheology of the materials. This motivates us to investigate the influence of interstitial liquid, that introduces cohesive forces into the materials, on the torque in the no aeration as well as in the fluidized state of dry and wet granular materials.

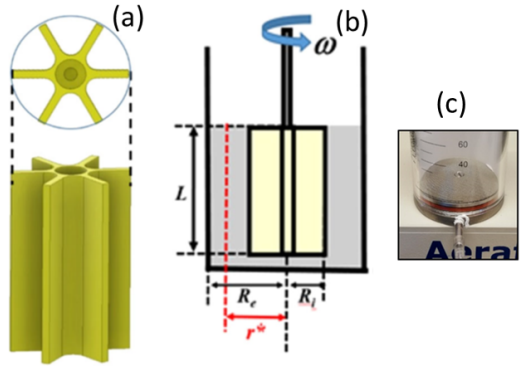

FIGURE 1 (a) Representative image of the 3D printed virtual Couette cell. (b) Schematic view of the assembled aerated bed virtual Couette rheometer (AB-VCR) with L beign the cell's height, ω the rotational speed, R_e, R_i and r^* the external, inner, and optimal radii, respectively. (c) stainless steel aeration base [24].

2 | EXPERIMENTAL APPARATUS

The aerated bed Virtual Couette Rheometer (VCR) consists of the combination of the aeration vessel of the automated Freeman FT4 Powder Rheometer (Freeman Tech.) and a cylindrical cell displaying six blades (3D printed cell) as shown in Figure 1(a, b). The aerated vessel of the FT4 is made up of a 25 mm inner radius (R_e) glass cylinder that can hold upto a volume of 260 cm^3. A stainless steel attachment is used as a base for the glass vessel bottom for aerated granular material tests (Figure 1(c)). The air flowing through the vessel is controlled by the FT4 air supply that assures air velocities up to 40 mm/s. The apparatus used, specifically, the geometry of the impeller is like that in the case studied by Ait Ali Yahia et al. [24] and Marchal et al. [15]. A detailed description of the VCR apparatus is given in Ait Ali Yahia et al. While Ait Ali Yahia et al. used 3D printed cell of variable lengths and radius, we used a cell of length $L = 70$ mm and radius $R_i = 15$ mm in this work. Note, that some preliminary experiments are done in aerated bed in the apparatus without the 3D printed cell to investigate the samples' behaviour in this condition.

3 | EXPERIMENTAL PROCEDURE

3.1 | Sample preparation

The experiments are done for two different glass beads sizes; (i) $d_p < 106\ \mu$m and (ii) $d_p \approx 150 - 212\ \mu$m, respectively. Initially, a dry sample is prepared by weighing out 200 g of glass beads powder. This mass of material is sufficient to immerse the impeller completely into the powder bed. The experiment is run without any further preparation for the dry sample following the methodology as explained in section 3.3.

For preparing samples of wet granular materials, liquid (silicon oil) of required volume is initially added to the 200 g of glass beads powder. The liquid content is varied systematically and added to the glass powder samples by means of pipette to analyse the system for varying range of cohesivity of powder. A conditioning cycle is then run using a regular stainless steel impeller blade supplied with the FT4 rheometer to mix the liquid with the glass powder and prepare the sample for wet granular experiments prior to the VCR experiments. The conditioning cycle traverse through the sample clockwise and anti-clockwise direction for 20 cycles to achieve homogeneity upon addition of the liquid. The impeller blade was then switched out and replaced by the 3D printed impeller. Thereafter, we performed the VCC experimen-

tal procedure with 3D printed cell as explained in section 3.3.

To study the effect of glycerol saturation, we analyse the wet powder samples with the glycerol volumes added to powder, varying from 0 to 70 μL with an interval of 10 μL. The corresponding saturation of silicon oil is $S^* \in (0 - 0.034)\%$, where S^* is the ratio of mass of liquid silicon oil to mass of solid glass powders, assuming that the density of silicon oil is 0.97 g/cm^3. In general, in the geophysics community, the pore saturation is commonly defined as the ratio of the liquid volume to the pore volume [1, 6, 9] and is denoted by S here. The regime of saturation for the arrangement of liquid bridges corresponding to the pendular mode of distribution is ambiguous and is suggested differently in various literatures. For example, Denoth suggested the regime of pore saturation for pendular mode of liquid bridges is $S < 11\%$ [1] while Weigert & Ripperger suggested the same for $S < 30\%$ [6, 9]. However, it is to be noted that the saturation for pendular regime as suggested by these studies are all with water as the interstitial liquid. We, however, have silicon oil as the interstitial liquid which has different interfacial properties. Nevertheless, we have silicon oil volume ranging from $0 - 70$ μL added to 200 g of glass beads and the corresponding pore saturation S is varying to less than 1%, assuming the bulk density of glass beads as 1.5 g/cm^3. Therefore, we assume that with this small pore saturation of silicon oil in the glass beads, we are in the pendular mode of distribution of liquid bridges.

3.2 | Shear test

In this section, we present an overview of the shear stress testing procedure and the details of the test performed using FT4 powder rheometer for different specimens of glass powders mixed with silicon oil. The purpose of the experiments in FT4 rheometer is to measure the bulk cohesion of the samples mentioned in section 3.1. Since the bulk cohesion of the samples play a fundamental role on the fluidization behaviour of the samples, we quantify the bulk cohesion for different samples by shear test method. The experimental equipment used in this work for doing the shear test is the FT4 Powder Rheometer (Freeman technology Ltd., UK), is same as the one used and demonstrated by Shi et. al [21]. Standard accessories for the shear test include a 50-mm-diameter blade for sample conditioning, a vented piston for compression, a shear head for the shearing process and a 50-mm-high with 50 mm diameter borosilicate test vessel. One advantage of the commercial FT4 Powder Rheometer is the automated nature of the procedure requiring minimal operator intervention.

The shear test sequence under the ASTM standard D7891 (ASTM-D7891-15, 2015) can be summarized as follows: the test vessel is carefully filled with the powder of interest using a spatula after obtaining the tare weight. The conditionig procedure involves the movement of the conditioning blade into the test sample to gently disturb the powder bed for a number of cycles before it is removed slowly. In this study, we perform three conditioning cycles before the shear tests are carried out. A cycle consists of the inward and outward movement of the conditioning blade into the powder bed with a constant rotation movement all the time. In order to prevent the conditioning blade from touching the base of the vessel, the direction of the blade movement is reversed as soon as it is within 1 mm of the vessel base. This creates a uniform, loosely packed test sample that can be readily reproduced [12].

In this study, we perform three pre-conditioning cycles before the shear tests are carried out. Subsequent to pre-conditioning, the blade is replaced with a vented piston, which incorporates a stainless steel mesh to allow the encosed air in the powder to escape uniformly across the surface of the powder bed. The vessel assembly is then split (and thus levelled) after the vented piston executes the compression until the pre-shear normal stress level is reached. Then the powder mass is recorded after splitting to compute the bulk density before the shear tests start. A detailed description of the vessel split-and-levelling procedure is reported by Freeman et al. (2009) [14].

A shear test begins after changing the vented piston to the shear head of the FT4 powder rheometer. The shear head moves downwards inserting the blades

into the powder and induces a normal stress as the shear head bottom surface is in contact with the top surface of the powder. The shear continues to move until the required pre-shear normal stress is reached. At this point slow rotation of the shear head begins, inducing an increasing shear stress. As the powder bed resists the rotation of the shear head, the shear stress increases until failure, at the point a maximum shear stress is observed. As a consequence. a shear plane is formed just below the ends of the blades. The shear head is kept moving until the shear stress does not change anymore for the pre-shear step and is stopped immediately after the maximum is reached for each shear step. A constant normal stress is maintained throughout each pre-shear or shear step. All tests performed with the FT4 powder rheometer follow ASTM standard.

The coefficient of internal friction and bulk cohesion for particle sizes $d_p < 106\,\mu$m and $d_p \approx 150-212\,\mu$m are evaluated for samples of varying silicon oil saturation using the shear test experiments and the values are reported in Table 1. As observed from the table, the coefficient of internal friction μ_s is independent of the saturation of silicon oil S^* for both particle sizes. However, the bulk cohesion c for both the particle sizes increase with increasing silicon oil saturation S^*. The definition of the two important strength parameters interpreted from the Mohr-Coulomb failure criterion explicate that the bulk cohesion c is the inherent strength of the materials arising from the cohesive forces between the structural elements and the coefficient of internal friction μ is the shear resistance arising from the frictional forces between the structural elements. While the frictional forces between constituent particles is primarily consistent with increasing saturation of silicon oil, the cohesive forces increase with increasing saturation in the pendular regime. Thus, μ is consistent while c increases with increasing amount of silicon oil added to the powder for the given range of saturation which is in the pendular regime. This is in agreement with the previous numerical studies on wet granular materials [18, 19]. Figure 2 shows the bulk cohesion as a function of the silicon oil saturation for particle sizes $d_p < 106\,\mu$m (blue $\triangle$ markers) and $d_p \approx 150 - 212\,\mu$m (red $\circ$ markers), respectively. As observed from the figure, the bulk cohesion of powders of both particle sizes increases with increasing amount of silicon oil.

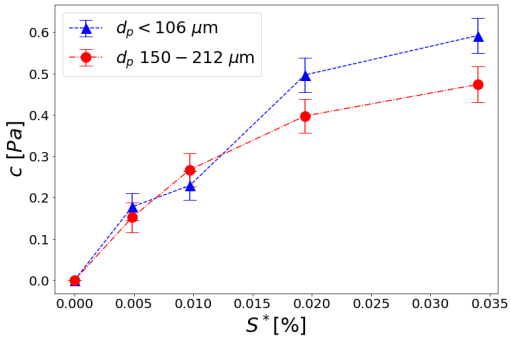

FIGURE 2 Shear test results for bulk cohesion as a function of silicon oil saturation for particle sizes $d_p < 106\,\mu$m (blue $\triangle$ markers) and $d_p \approx 150 - 212\,\mu$m (red $\circ$ markers).

3.3 | Experiments with 3D printed cell

The experimental procedure for VCR is as follows: the 3D printed cell moves downward through the material placed in the vessel until it reaches a fixed position, which, in the present study, is assumed to be constant and equal to 1 mm, measured from the bottom of the vessel. The granular material under investigation is first fluidized at high airflow to allow the cell to move downward. The pre-fluidization is done to avoid the cell to compact the sample which causes the device to be overloaded. Once the cell has reached the fixed position, the aeration is stopped and the arm holding the cell starts rotating at a fixed rotational speed, ω. The vessel is filled with enough material to cover the height of the cell. The torque, T, needed to rotate this cylinder through the bed of particles is recorded. This procedure is followed while we again start the aeration of the granular bed from the bottom of the bed and record the torque and pressure drop across the bed. Although, the experiments without the VCR for wet cohesive powders reveal inhomogeneous bed with formation of channels, the 3D printed cell in

TABLE 1 Steady state friction μ and bulk cohesion c for dry and wet powders.

Particle size $d_p < 106\ \mu$m			Particle size $d_p \approx 150 - 212\ \mu$m		
S^*[%]	μ	c **[Pa]**	S^*[%]	μ	c **[Pa]**
0	0.36	0	0	0.32	0
0.005	0.33	0.18	0.005	0.34	0.15
0.010	0.34	0.23	0.010	0.33	0.27
0.019	0.34	0.50	0.019	0.33	0.40
0.034	0.32	0.59	0.034	0.32	0.47

the current experiments rather homogeneously mix the bed and enable fluidization of the sample for small saturation of silicon oil. The experimental data with VCR are repeated several times to check the consistency and reproducibility of the results.

The stress is evaluated from the recorded torque, T, as follows:

$$\tau = K_\tau(r)T \text{ with } K_\tau(r) = \frac{1}{2\pi L r^{*2}} \tag{1}$$

where K_τ is the shear stress geometrical constant and L is the height of the cell. This constant is obtained by solving the equation of motion in case of a fluid obeying power law model in a Couette flow configuration, i.e. $\tau = v\dot{\gamma}^n$, where τ is the shear stress, v is the flow consistency index, $\dot{\gamma}$ is the shear rate or the velocity gradient perpendicular to the plane of shear and n is the flow index. It should be noted that the above equation is obtained while considering a uniform stress distribution along the height of the cell, L.

The shear rate $\dot{\gamma}$ is evaluated from the rotation rate as follows:

$$\dot{\gamma} = 2\frac{\left(R_e/r^*\right)^2}{\left(R_e/R_i\right)^2 - 1}\omega \tag{2}$$

where R_e is the inner radius of the glass apparatus, R_i is the radius of the 3D printed cell, r^* is the optimal radial position where the shear stress and shear rate are independent of the cell geometry and ω is the rotation rate of the 3D printed cell. From the analytical solutions of Eq.1 and 2, Ait-Kadi et al. derived that the optimal radius r^* depends on the cell geometry but is independent of the material characteristics [7]. The significance of the optimal radius as defined by Ait-Kadi et al. specifies that the shear rate $\dot{\gamma}$ is independent of the flow index n at the position r^* in the Couette cell. Thus, the optimal radius r^* gives a measure of the local shear rate which is independent of the type of fluid in the rheometer.

3.3.1 | Fluidization experiments

The fluidization experiments are conducted for varying saturation of silicon oil in the glass bead samples with the rotating cell in Couette rheometer. For cohesive powders, the limit of fluidization is reached if the drag forces exerted from the percolating gas on the particles within the regime of fluidization do not exceed the adhesion forces between the particles, thus not resulting in break up of the fixed bed structure. A non-dimensional group which defines the limit of fluidization, is obtained by division of maximum drag force by the average tensile force on the particles [2]. The rotating cell in the Couette rheometer contributes to additional inertial forces to the particles, thus extending the fluidization limit of the cohesive particles. The fluidization limit is then obtained from the ratio of the drag and inertial forces to the average tensile forces on the particles [3]. Thus, introducing a rotating cell in the Couette rheometer during fluidization increases the fluidization limit of the cohesive particles. The rotation rate is kept fixed at $\omega = 40$ rpm for the

fluidization experiments. The air flow rate is systematically increased in the experiments while the measured shear stress decreases with air flow. The air flow rate U is varied from $0-40$ mm/s for particle sizes $d_p < 106\,\mu$m and from $0-80$ mm/s for particle sizes $d_p \approx 150-210\,\mu$m. A smaller step size is chosen for the incremental air flow for smaller size particles $d_p < 106\,\mu$m as compared to the particle sizes $d_p \approx 150-210\,\mu$m in order to obtain a better resolution of the results at small fluidization velocities. The air flow rate is decreased in just the reverse order for the de-fluidization experiments.

3.3.2 | Rheology in aerated bed

The experiments on rheology in aerated bed are done for two different particle sizes $d_p < 106\,\mu$m and $d_p \approx 150-210\,\mu$m, respectively. The experiments are conducted with the rotation rates of the 3D printed impeller ω varying from $0-120$ rpm. The whole set of rheology experiments are done for four samples; dry non-cohesive powders and wet cohesive powders with $S^* = 0.005$, respectively, for two different particle sizes and the results are compared.

4 | RESULTS

4.1 | Fluidization

The purpose of this study is to examine the effect of interstitial liquid, e.g. silicon oil in powders, on the fluisation behaviour of the unsaturated wet powders. For this analysis, we vary the amount of silicon oil in the powder and analyse the pressure drop through the bed for varying air flow rate through the bed. We also do our studies for powders of two different particle sizes, $d_p < 106\,\mu$m and $d_p \approx 150-212\,\mu$m, respectively. For the present study, the experimental procedure presented in 3.3.1 is performed for different saturation of the wet samples with varying air flow rates in the bed for two different glass bead samples of sizes of $d_p < 106\,\mu$m and $d_p \approx 150-212\,\mu$m, respectively.

Figure 3(a) illustrates the effect of silicon oil saturation on the evolution of the pressure drop across the bed of the materials as a function of the superficial air velocity for particle size $d_p < 106\,\mu$m. Most notably, experiments without silicon oil or with a very weak saturation of silicon oil ($S^* = 0.005\%$) show a very small pressure drop overshoot. The plot shows that the pressure drop corresponding to dry materials and weakly cohesive wet materials ($S^* = 0.005\%$) in the steady state approximately 10 mbar balances the materials' weight of 200 g reaching a fluidized state. Unlike dry and weakly saturated materials, experiments with increasing silicon oil saturation show a clear pressure drop overshoot. This suggests that bulk cohesion in wet materials is a factor leading to the overshoot of the pressure, indicating that the supplemental pressure drop is due to the breakage of interparticle cohesive forces as air flows through the bed. With further increase in air velocity, the peak pressure starts to decay and finally reaches a constant value of pressure drop across the bed. However, this pressure drop in the steady state does not balance the weight of the materials, suggesting that the material is not fluidized. Notably, the pressure drop overshoot as well as in the steady state increases with increasing saturation of silicon oil due to the effects of interparticle cohesive forces. The additional pressure drop in the steady state for cohesive materials is a result of the air flow through the materials breaking the interparticle cohesive forces.

Figure 3(b) illustrates the effect of silicon oil saturation on the evolution of the pressure drop across the bed of the materials as a function of the superficial air velocity for particle size $d_p \approx 150-212\,\mu$m. The results are similar to the observations related to smaller particle sizes $d_p < 106\,\mu$m. However, unlike the smaller particles, here we do not observe a sharp overshoot in the pressure. Figure 4(a) shows a sample of $d_p \approx 150-212\,\mu$m with weakly saturated silicon oil ($S^* = 0.005\%$). As observed from the figure, bubbles are formed near the free surface, making the surface uneven. Figure 4(b) corresponds to a sample of $d_p \approx 150-212\,\mu$m with higher saturation of silicon oil ($S^* = 0.034\%$). In contrast to the Figure 4(a), in Figure 4(b) we observe channels are formed within the materials and the sample is not fluidized.

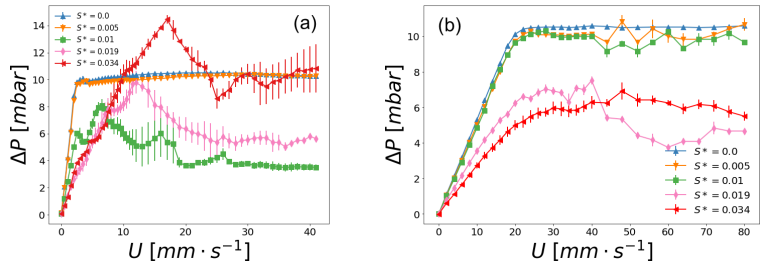

FIGURE 3 Pressure drop as a function of superficial air velocity for powders of varying glycerol saturation and particle size (a) $d_p < 106\ \mu$m and (b) $d_p \approx 150 - 212\ \mu$m with varying amount of silicon oil added.

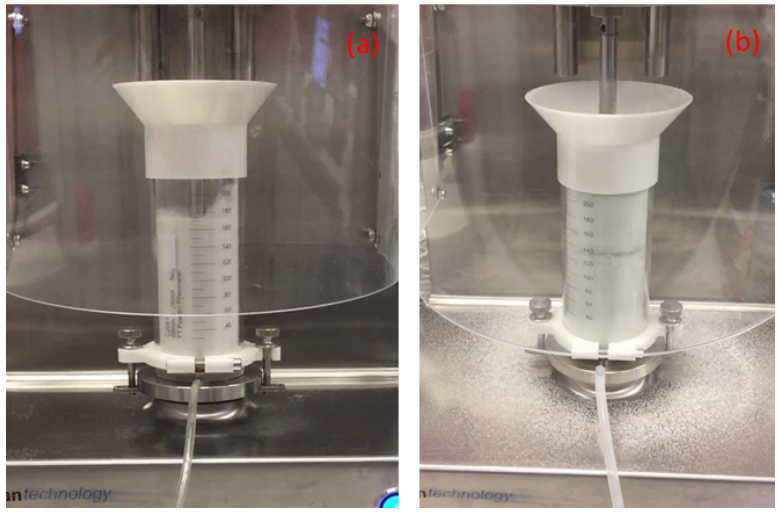

FIGURE 4 Snapshots of experiments for particle size $d_p \approx 150 - 212\ \mu$m tests in VCR showing (a) fluidization of weakly cohesive powder ($S^* = 0.005\%$) and (b) cohesive powder ($S^* = 0.019\%$) that is not fluidized.

4.2 | Fluidization Vs de-fluidization

The primary focus of this effort is to examine how cohesive forces affect the fluidization and de-fluidization behaviour for dry and wet powders. The objective is to see if the fluidization and de-fluidization follow the same path or there is a hysteresis that exists in the path and under which circumstances. As observed in Section 4.1, powders of particle size $d_p < 106\ \mu$m do not fluidize for $S^* > 0.005$ and that of particle size $d_p \approx 150 - 212\ \mu$m do not fluidize for $S^* > 0.01$. For powders that do not fluidize, we focus on studying their aeration and de-aeration behaviour. For the present study, the experimental procedure presented in 3.3.1 is performed for three different saturation of the samples, $S^* 0, 0.005\%$ and 0.019%, respectively, with varying air flow rates through the bed, for two different glass bead samples of sizes of $d_p < 106\ \mu$m and $d_p \approx 150 - 212\ \mu$m, respectively.

During the fluidization and de-fluidization cycle, the pressure drop is measured to get an insight into the impact of cohesive forces on the fluidization behaviour of wet powders of particle size $< 106\ \mu$m. Observations

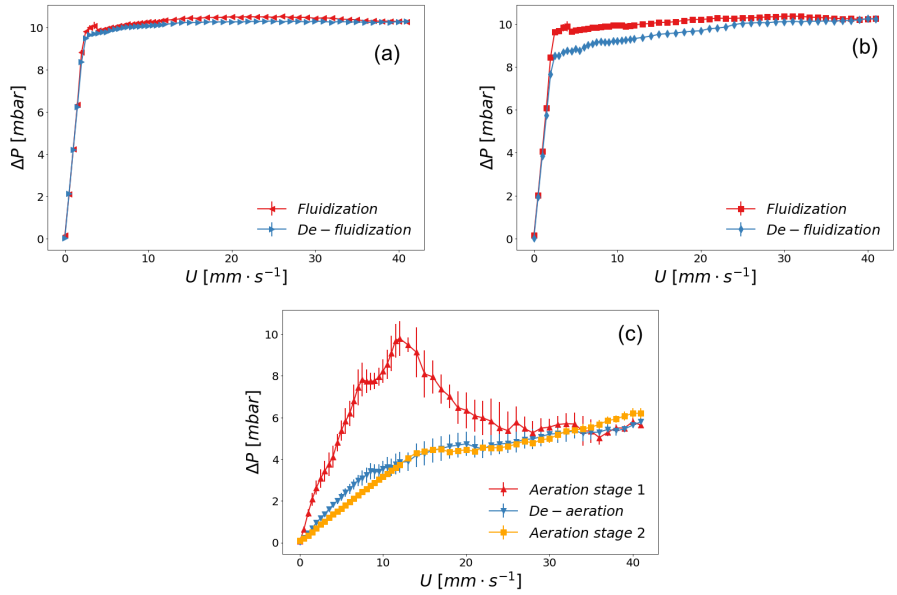

FIGURE 5 Fluidization and de-fluidization curves for powders of glycerol saturation (a) $S^* = 0\%$, (b) $S^* = 0.005\%$ and (c) aeration and de-aeration curves for powder of glycerol saturation $S^* = 0.019\%$ for particle size $d_p < 106\ \mu$m.

from Figure 5 reveal that the extent of hysteresis in the cycle also increases with increasing cohesion effect. The pressure drop curve during de-fluidization lies well below that for fluidization. This behaviour is in good agreement with the earlier DPM-CFD studies done by Galvin et al. [17]. Figure 5(a) shows that the fluidization (red line) and de-fluidization (blue line) curves track one another closely and only a slight hysteresis is evident for the dry free flowing materials. For intermediate cohesion, as shown in Figures 5(b), the de-fluidization curve deviate from the fluidization and the hysteresis effect increases with increasing powder cohesion. For even higher cohesion, when the particle bed can not be fluidized and we here analyse the path of aeration and de-aeration of the materials. The hysteresis effect increases further as shown in Figure 5(c) compared to the fluidization and defluidization of samples in Figures 5(a) and (b). This hysteresis effect can be related to the changes in voidage of the bed during de-aeration, i.e. the granular bed is denser during first aeration process than that after following de-aeration for cohesive powders. We verified this fact by continuing aeration (indicated by aeration stage 2) after de-aeration, which gives similar trend as shown in Figure 5(c). The orange and blue lines agree well, indicating that the second aeration follows a different path than the first and hence has a different bed condition.

Similar results are obtained for particle size $d_p \approx 150 - 212\ \mu$m. Figure 6(a) and (b) show the fluidization and de-fluidization curves for dry free flowing and weakly cohesive wet powders, respectively, for particle size 150–212 μm. Observations from Figure 6(b) also suggests that the extent of hysteresis in the fluidization and de-fluidization cycle also increases with increasing cohesion effect, similar to observations for particle size $d_p < 106\ \mu$m in Figure 5(b). Figure 6(c) shows the aeration/ de-aeration curve for higher cohesive wet powders and here the hysteresis effect increases even more but the bed is not fluidized.

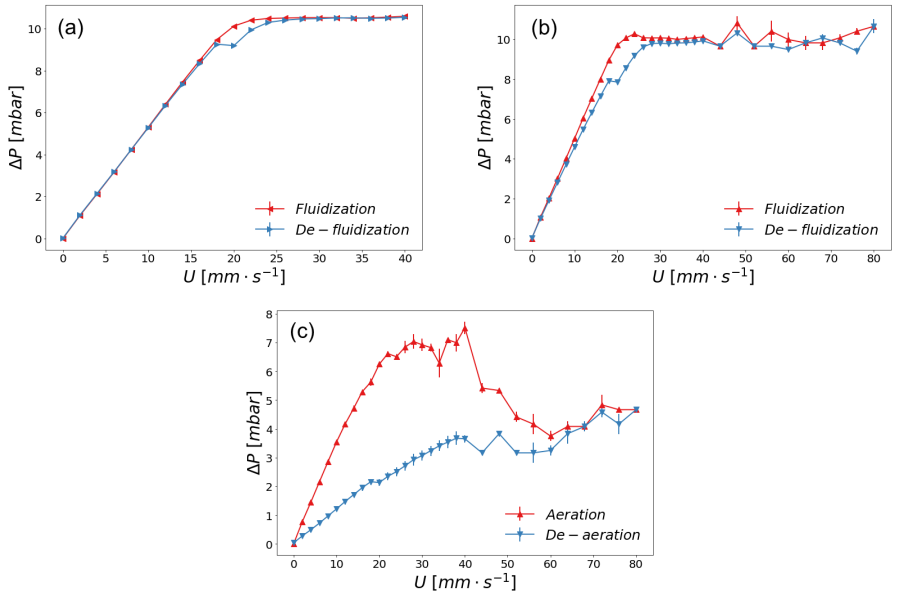

FIGURE 6 Fluidization and de-fluidization curves for powders of glycerol saturation (a) $S^* = 0\%$, (b) $S^* = 0.005\%$ and (c) aeration and de-aeration curves for powder of glycerol saturation $S^* = 0.019\%$ for particle size $d_p \approx 150 - 212\ \mu$m.

4.3 | Shear stress of materials in aerated bed

The torque is an experimentally accessible quantity that can be measured in the Couette cell which gives an evaluation of the shear stress or bulk cohesion of the material [19]. The bulk cohesion is a measure of the inherent strength of the materials which is clearly a function of the liquid saturation in the powder. Thus, measuring the torque gives an estimation of the strength of the dry or wet materials during fluidization. Therefore, we calculate the shear stress from the experimentally measured torque and look into their behaviour as a function of fluidization velocity. The model used to calculate the shear stress from the recorded torques is given in Equation 1. For the present study, the experimental procedure presented in 3.3.1 is performed for different saturation of the wet samples with varying air flow rates in the bed for two different glass bead samples of sizes of $d_p < 106\ \mu$m and $d_p \approx 150 - 212\ \mu$m, respectively.

As observed from Figure 7(a), the steady state shear stress decreases monotonically as a function of air flow velocity for particle sizes $< 106\ \mu$m. Further, for a given air flow velocity, the shear stresses consistently increases with increasing saturation of silicon oil in the powder. In addition, we have processed the results further to identify trends for normalised stress as a function of the air velocity U as shown in Figure 7(b). The normalised stress is obtained by normalising the shear stress of wet materials, τ_w, by the shear stress of dry materials, τ_d, at the same air flow velocity. The normalised shear stress increases with wet powder cohesion as the saturation of silicon oil in the powder increases. For each trend corresponding to a wet powder sample, the normalised shear stress initially increases due to the passage of air through cohesive materials and reaches a peak value. With further increase in air velocity U, the normalised shear stress decreases due to the breaking of cohesive force bonds and finally approaches the shear stress value as of the dry free flowing powder.

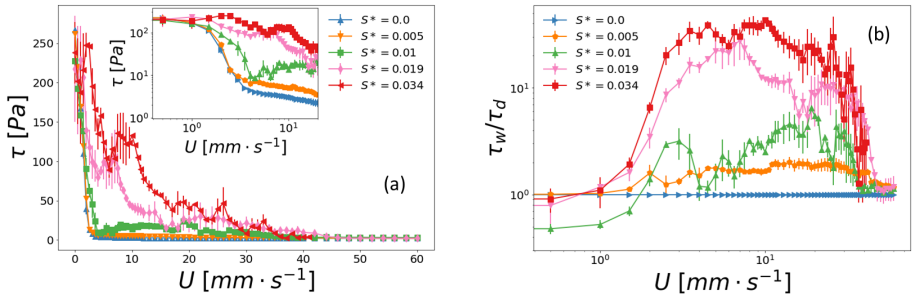

FIGURE 7 (a) Shear stress as a function of air velocity and (b) non-dimensional shear stress τ_w/τ_d as a function of superficial air velocity for dry non-cohesive and wet cohesive particles size $d_p < 106\ \mu$m with varying saturation of silicon oil S^* added.

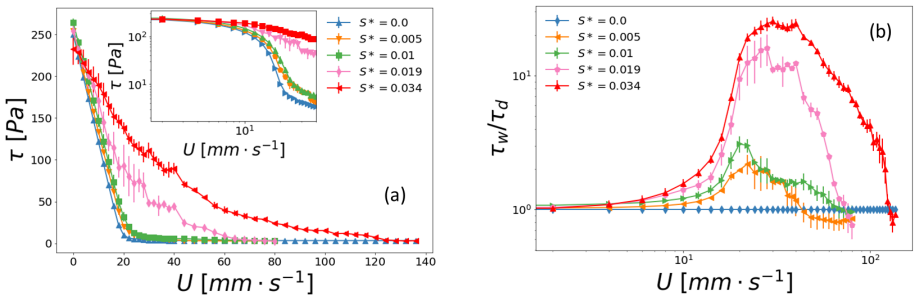

FIGURE 8 (a) Shear stress as a function of air velocity and (b) non-dimensional shear stress τ_w/τ_d as a function of superficial air velocity for dry non-cohesive and wet cohesive particles size $d_p \approx 150 - 212\ \mu$m with varying saturation of silicon oil S^* added.

Figure 8(a) shows the yield shear stress for particle size d_p 150 − 212 μm. Similar to the behaviour shown by particle size < 106 μm, the shear stress here also decreases monotonically as a function of the air flow velocity. The shear stress for a given air flow velocity increases with increasing saturation of silicon oil. The normalised shear stress increases with wet powder cohesion as the saturation of silicon oil in powder increases as shown in figure 8(b). The trends corresponding to each wet powder sample is similar to that exhibited by the wet powder particle size $d_p < 106\ \mu$m. The normalised shear stress initially increases, reaches a peak value and then decreases as a function of increasing air flow velocity.

4.4 | Rheology of granular materials in aerated bed

In this section, we analyse the shear stresses of dry and wet powders as a function of the shear rates in the steady state rotation of the cell. The stress-shear rate analysis is a prerequisite for developing constitutive relations for new materials and thus this provides the motivation for these analyses. The model used to calculate the shear stress and shear rates from the recorded torques and the rotational speeds are given in Equation 1 and Equation 2, respectively. The time evolution of the recorded torque is shown and we only focus here on the steady state torque for varying rotation rates of the cell and varying silicon oil content for both particle sizes $d_p < 106\ \mu$m

and $d_p \approx 150 - 212\ \mu$m.

The shear stresses are evaluated from the torque and the results are plotted in Figure 9(a) and (b) for particle sizes $d_p < 106\ \mu$m and $d_p \approx 150 - 210\ \mu$m, respectively. The results show stresses for both dry and wet powders, represented by the solid and dash-dotted lines, respectively. For the present study, the experimental procedure presented in 3.3.2 is performed for various rotation rates of the 3D printed impeller with dry samples and wet samples of saturation of silicon oil $S^* = 0.005\%$ for two different glass bead samples of sizes of $d_p < 106\,\mu$m and $d_p \approx 150-212\,\mu$m, respectively. The fluidization index is defined as the ratio of the pressure drop across the bed to the weight of the material per unit area of cross-section, i.e. $FI = \Delta PA/mg$. The air velocities are adjusted for different samples to maintain constant pressure drop across the bed for a specified FI. Prior to performing experiments with wet glass beads powders, we perform experiments with dry powders and verify our results with Ait Ali Yahia et al. [24]. The results presented in Figure 9(a) and (b) show that for all the powder samples studied, the shear stress is independent of the shear rate. The experiments are performed in the quasi-static regime where the friction coefficient is independent of the shear rate. Further, it is observed that the shear stress decreases as the FI increases. These observations for experiments with dry powders are quantitatively agreeing with the results of Ait Ali Yahia et al. [24]. The results presented in the figure also show that when the particles are aerated, the shear stress decreases as FI increases. The decrease in shear stress with increasing FI is explained by the fact that when aerated, the pressure acting on the particles decreases, which leads to a decrease in viscosity. Thus, at a fixed shear rate, the shear stress decreases as the FI increases. This is also explained by the fact that when aerated, the pressure acting on the particles decreases, which leads to a decrease in shear stress. The average shear stress over the studied shear rates is evaluated for each FI for different particle sizes $d_p < 106\ \mu$m and $d_p \approx 150 - 210\ \mu$m. The shear stress corresponding to cohesive materials are consistently higher than the non-cohesive ones for the same fluidized bed conditions. This is more evident since cohesive materials have additional attractive forces between particles which contributes to additional shear stress while shearing.

The solid viscosities are evaluated as the ratio of shear stress to shear rate and the results are plotted in figure 10(a) and (b) for particle sizes $d_p < 106\ \mu$m and $d_p \approx 150 - 210\ \mu$m, respectively. The results show viscosities for both dry and wet powders, represented by the solid and dash-dotted lines, respectively. The viscosity decreases with increasing the shear rate following a power law fit with slope equal to -1 for both free flowing and cohesive powders. This corresponds to a Coulomb behavior which was also observed by Marchal et al. [15] using a similar cell configuration. Similar results were also shown numerically by Luding [13] where the trend of viscosity decreases linearly with the non-dimensional Inertial number with a slope of -1 in the region of higher pressure in the bulk of the materials. The results presented in Figure 10(a) and (b) also show that the viscosity is consistently higher for wet cohesive powders as compared to dry free flowing powders corresponding to the same FI for both particle sizes $d_p < 106\ \mu$m and $d_p \approx 150 - 210\ \mu$m. This is also more evident since cohesive materials have higher shear rate compared to dry free-flowing materials at a given shear rate.

5 | CONCLUSIONS

The fluidization behaviour of dry free flowing and wet cohesive powders are studied for different cohesion intensity in a Virtual Couette Cell. This new rheometer which was developed by Ait Ali Yahia et al. to measure the fluidization behaviour and bulk solid stresses of dry granular materials in an aerated bed, is here extended to measure and compare the fluidization behaviour of both dry free flowing and wet cohesive powders.

Experiments on fluidization of dry free flowing powders show a very small pressure overshoot for both particle sizes. Unlike dry free flowing materials, experiments with cohesive powders with increasing silicon oil satu-

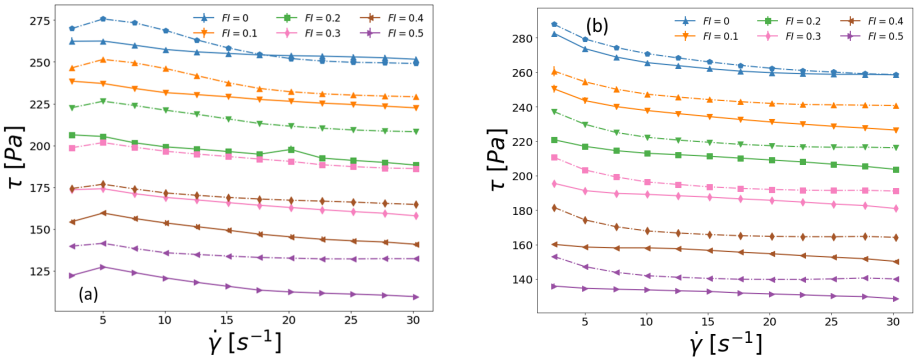

FIGURE 9 Shear stress as a function of shear rate at various FIs: (a) $d_p < 106\ \mu$m and (b) $d_p \approx 150 - 212\ \mu$m. The plots corresponding to different colors are for experiments with different fluidization Index (FI) as shown in the legends. For plots corresponding to a given colour, the solid lines correspond to the shear stress for dry non-cohesive materials and the dash-dotted lines correspond to cohesive materials with silicon oil saturation $S^* = 0.005\%$ for the same FI.

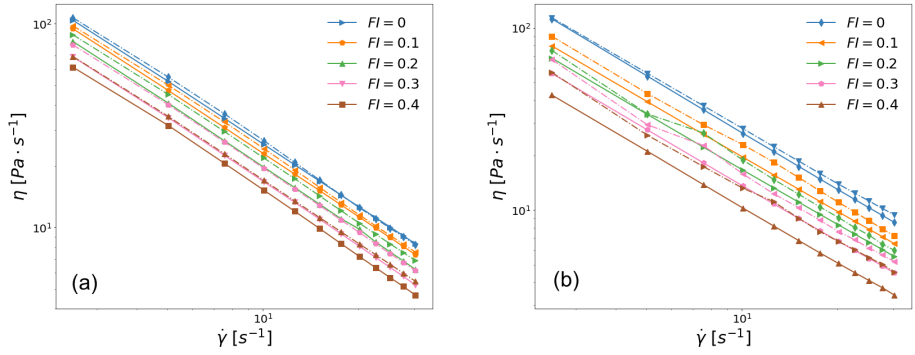

FIGURE 10 Viscosity as a function of shear rate at various FIs: (a) $d_p < 106\ \mu$m and (b) $d_p \approx 150 - 212\ \mu$m. The plots corresponding to different colors are for experiments with different fluidization Index (FI) as shown in the legends. For plots corresponding to a given colour, the solid lines correspond to the shear stress for dry non-cohesive materials and the dash-dotted lines correspond to cohesive materials with silicon oil saturation $S^* = 0.005\%$ for the same FI.

ration show a clear pressure overshoot, especially for small particle size. While dry free flowing and weakly cohesive materials reach a fluidized state, higher cohesive materials can not be fluidized. For dry and weakly cohesive materials in the fluidized state, the pressure drop is approximately balanced by the weight of the materials. For intermediate and higher cohesive materials, the materials' weight is not balanced by the steady state pressure drop.

The extent of hysteresis in the fluidization and de-fluidization cycle increases with increasing cohesion effect. While the fluidization and de-fluidization curves track one another closely and only a slight hysteresis is observed for dry free flowing powders, the hysteresis

effects in the cycle increases with increasing cohesion effects. For higher cohesive materials, the hysteresis effect increases even more but the bed is not fluidized. This is due to a different granular voidage condition that is created during de-aeration. This fact is verified by continuing aeration after de-aeration that follows a different path than the initial aeration process, indicating the existence of a different bed condition than initially.

The steady state shear stress decreases monotonically as a function of air flow velocity for both dry and wet powders. Further, the shear stresses for cohesive powders are consistently higher than the dry free flowing powders at a given gas velocity. The normalised shear stress increases with increasing saturation of silicon oil for cohesive powders. For a given cohesive powder sample, the normalised shear stress initially increases due to the passage of air through the powder sample, breaking the inter-particle capillary bridges. With further increase in air velocity, the normalised shear stress decreases and finally approaches the shear stress of dry free flowing powder once the cohesive bonds are broken.

The rheology experiments are conducted in the quasistatic regime and the shear stresses are nearly independent of the shear rate for both dry and wet granular materials. The stresses of the wet cohesive materials are consistently higher than the dry free flowing materials under the same pressure drop condition in the fluidized bed. The granular viscosity plots show that it decreases linearly as a function of shear rate with a slope -1, indicating that both dry and wet powders exhibit Coulomb behaviour.

ACKNOWLEDGEMENT

Financial support from the EPSRC is kindly acknowledged.

SYMBOLS AND ABBREVIATIONS

- d_p particle diameter (μm)
- c bulk cohesion (Pa)
- μ coefficient of internal friction
- τ shear stress (Pa)
- τ_w shear stress of wet materials (Pa)
- τ_d shear stress of dry materials (Pa)
- V volume of silicon oil (μL)
- S^* saturation of silicon oil
- K geometrical factors (rad^{-1})
- L cell height (mm)
- n flow index
- ΔP pressure drop across bed (mbar)
- r radial position (mm)
- r^* optimal radial position (mm)
- R_i inner radius (mm)
- R_e external radius (mm)
- FI fluidization index
- m mass of materials (g)
- g acceleration due to gravity (cm/s^2)
- A area of cross-section of bed (cm^2)
- U air velocity (mm/s)
- $\dot{\gamma}$ shear rate (s^{-1})
- η viscosity (Pa/s)

References

[1] A Denoth. “The pendular-funicular liquid transition in snow”. In: *Journal of Glaciology* 25.91 (1980), pp. 93–98.

[2] O Molerus. “Interpretation of Geldart’s type A, B, C and D powders by taking into account interparticle cohesion forces”. In: *Powder technology* 33.1 (1982), pp. 81–87.

[3] R Chirone, L Massimilla, and S Russo. “Bubble-free fluidization of a cohesive powder in an acoustic field”. In: *Chemical Engineering Science* 48.1 (1993), pp. 41–52.

[4] P Anjaneyulu and DV Khakhar. “Rheology of a gas-fluidized bed”. In: *Powder Technology* 83.1 (1995), pp. 29–34.

[5] Gabriel I Tardos, M Irfan Khan, and David G Schaeffer. “Forces on a slowly rotating, rough cylinder in a Couette device containing a dry, frictional powder”. In: *Physics of Fluids* 10.2 (1998), pp. 335–341.

[6] Tom Weigert and Siegfried Ripperger. “Calculation of the liquid bridge volume and bulk saturation from the half-filling angle”. In: *Particle & Particle Systems Characterization: Measurement and Description of Particle Properties and Behavior in Powders and Other Disperse Systems* 16.5 (1999), pp. 238–242.

[7] Abdellatif Aıt-Kadi et al. “Quantitative analysis of mixer-type rheometers using the Couette analogy”. In: *The Canadian Journal of Chemical Engineering* 80.6 (2002), pp. 1166–1174.

[8] Jens Klein, Detlef Höhne, and Klaus Husemann. “The influence of air permeation on the flow properties of bulk solids”. In: *Chemical Engineering & Technology: Industrial Chemistry-Plant Equipment-Process Engineering-Biotechnology* 26.2 (2003), pp. 139–146.

[9] Namiko Mitarai and Franco Nori. “Wet granular materials”. In: *Advances in Physics* 55.1-2 (2006), pp. 1–45.

[10] Diego Barletta et al. “A rotational tester for the characterization of aerated shear flow of powders”. In: *Particle & Particle Systems Characterization* 24.4-5 (2007), pp. 259–270.

[11] Giovanna Bruni et al. “A rheological model for the flowability of aerated fine powders”. In: *Chemical Engineering Science* 62.1-2 (2007), pp. 397–407.

[12] R. Freeman. “Measuring the flow properties of consolidated, conditioned and aerated powders-A comparative study using a powder rheometer and a rotational shear cell”. In: *Powder Technology* 174.1-2 (2007), pp. 25–33.

[13] Stefan Luding. “The effect of friction on wide shear bands”. In: *Particulate Science and Technology* 26.1 (2007), pp. 33–42.

[14] R. Freeman. “Measuring shear properties and normal stresses generated within a rotational shear cell for consolidated and non-consolidated powders”. In: *Powder Technology* 174.1-2 (2009), pp. 65–69.

[15] Ph Marchal, N Smirani, and L Choplin. “Rheology of dense-phase vibrated powders and molecular analogies”. In: *Journal of Rheology* 53.1 (2009), pp. 1–29.

[16] Igino Tomasetta et al. “The measurement of powder flow properties with a mechanically stirred aerated bed”. In: *Chemical Engineering Science* 69.1 (2012), pp. 373–381.

[17] Janine E Galvin and Sofiane Benyahia. “The effect of cohesive forces on the fluidization of aeratable powders”. In: *AIChE Journal* 60.2 (2014), pp. 473–484.

[18] Sudeshna Roy, Stefan Luding, and Thomas Weinhart. “Macroscopic bulk cohesion and torque for wet granular materials”. In: *The 8th International Conference for Conveying and Handling of Particulate Solids*. 2015.

[19] Sudeshna Roy et al. “Micro–macro transition and simplified contact models for wet granular materials”. In: *Computational particle mechanics* 3.4 (2016), pp. 449–462.

[20] Hamid Salehi et al. “Experiments and simulation of torque in Anton Paar powder cell”. In: *Particulate Science and Technology* 36.4 (2018), pp. 501–512.

[21] Hao Shi et al. “Effect of particle size and cohesion on powder yielding and flow”. In: *KONA Powder and Particle Journal* (2018), p. 2018014.

[22] Abbas Kamranian Marnani et al. “The Effect of the Presence of Very Cohesive Geldart C Ultra-Fine Particles on the Fluidization of Geldart A Fine Particle Beds”. In: *Processes* 7.1 (2019), p. 35.

[23] Mohammad Asif et al. “Hydrodynamics of Pulsed Fluidized Bed of Ultrafine Powder: Fully Collapsing Fluidized Bed”. In: *Processes* 8.7 (2020), p. 807.

[24] Lyes Ait Ali Yahia et al. “Development of a virtual Couette rheometer for aerated granular material”. In: *AIChE Journal* 66.6 (2020), e16945.

[25] Lizhuo Zhu et al. “Triggering flow of jammed cohesive granular materials using modulated pulsed airflow”. In: *AIChE Journal* 68.1 (2022), e17411.